1 **SUPPLEMENTAL FIGURES, TABLE, AND METHODS**
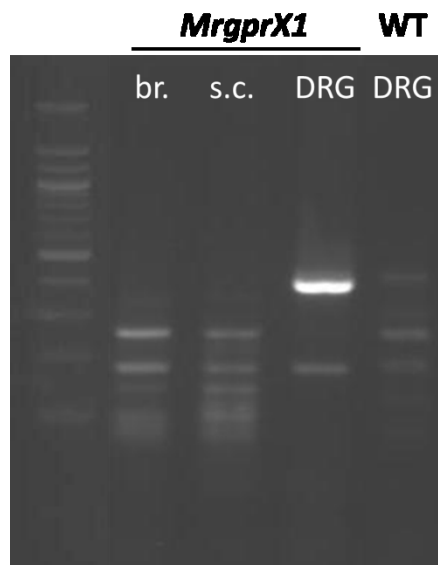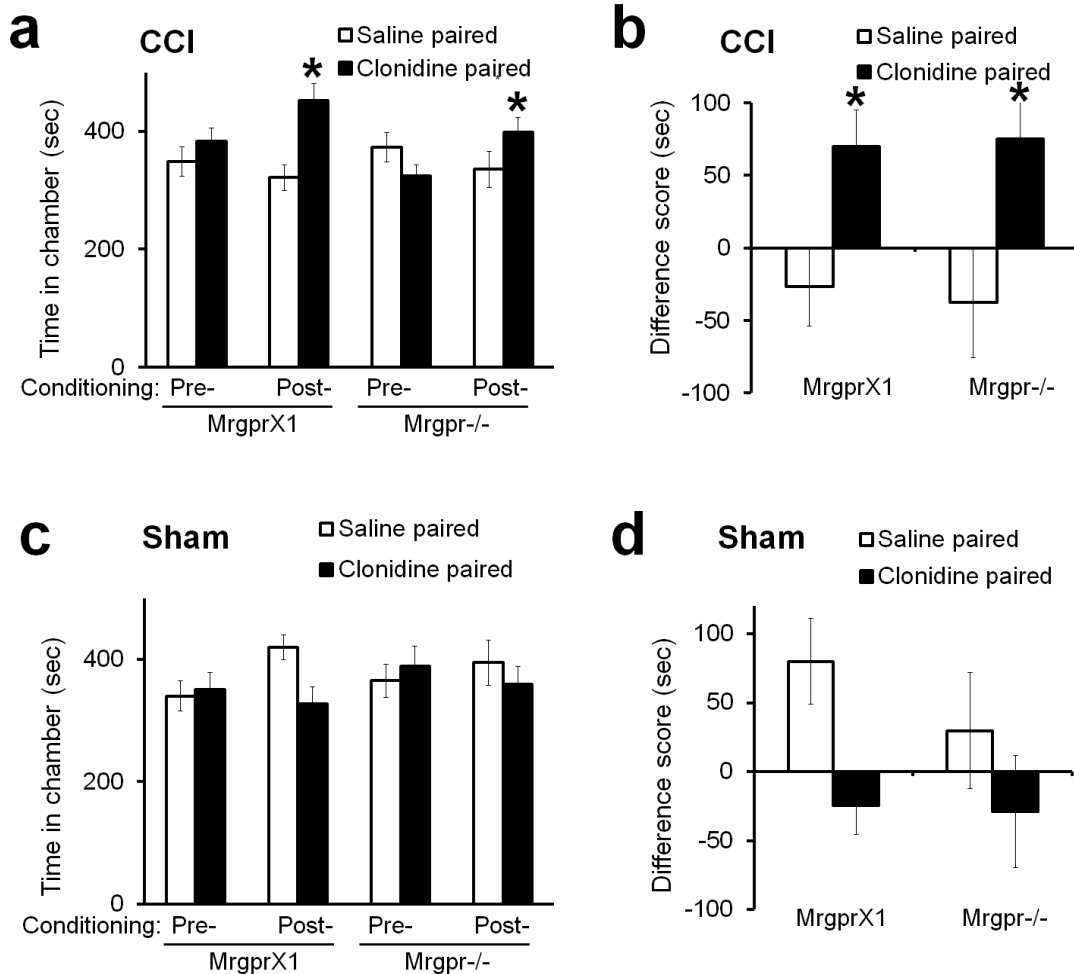

2

3 **SI Appendix, Fig. S1. The expression of *MrgprX1* mRNA in the DRG of humanized**

4 **MrgprX1 mice.**

5 Reverse transcript PCR shows the expression of *MrgprX1* mRNA in dorsal root ganglion

6 (DRG) neurons but not in brain or spinal cord. br.=brain, s.c.=spinal cord, ctrl = DRGs

7 from wildtype (WT) littermate without *MrgprX1* transgene.

8

9

10

a

CCI

☐ Saline paired
■ Clonidine paired

Graph showing Time in chamber (sec) vs Conditioning for MrgprX1 and Mrgpr-/- groups

b

CCI

☐ Saline paired
■ Clonidine paired

Graph showing Difference score (sec) for MrgprX1 and Mrgpr-/-

c

Sham

☐ Saline paired
■ Clonidine paired

Graph showing Time in chamber (sec) vs Conditioning for MrgprX1 and Mrgpr-/- groups

d

Sham

☐ Saline paired
■ Clonidine paired

Graph showing Difference score (sec) for MrgprX1 and Mrgpr-/-

1

SI Appendix, Fig. S2. Positive control of conditioned place preference induced by clonidine after nerve injury.

(a) Intrathecal administration of clonidine (1 µg, 5 µL saline) induced chamber preference in both *MrgprX1* and *Mrgpr-/-* mice at day 7–13 after chronic constriction injury (CCI) of sciatic nerve (*n*=12/group). *$P<0.05$ vs pre-conditioning. **(b)** The difference score analysis confirmed that both genotypes showed preference for the clonidine-paired chambers. *$P<0.05$ vs. saline. **(c)** The same dose of clonidine did not induce chamber preference in sham-operated mice, regardless of genotype (*n*=12/group). **(d)** The difference score confirmed that neither genotype showed a preference for the clonidine-paired chamber. a,c: Two-way repeated measures ANOVA, with Bonferroni *post hoc* test. b.d: Paired t-test.

2

1
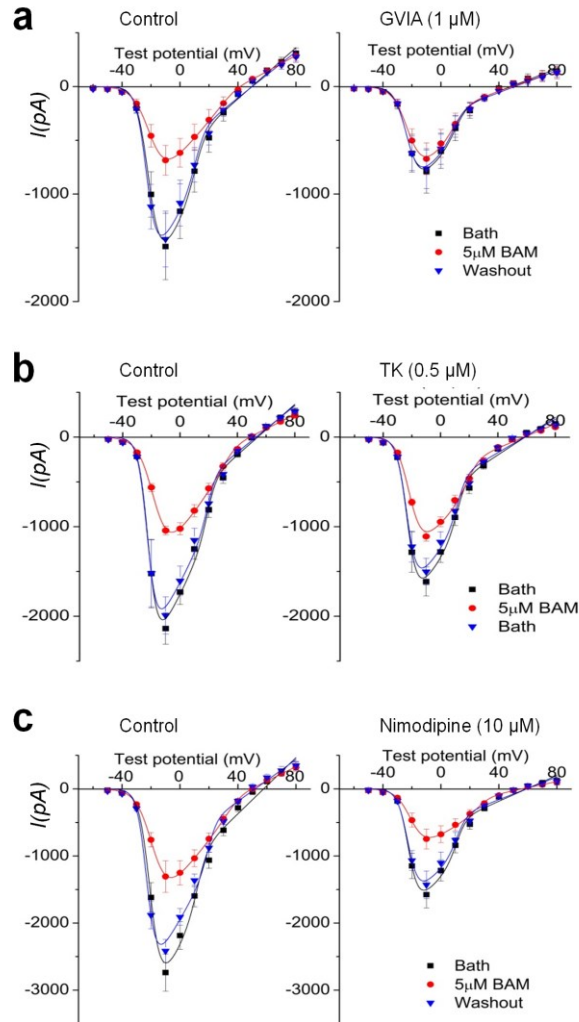
SI Appendix, Fig. S3. Examples of BAM8–22-induced inhibition of different types of high-voltage-activated (HVA) I_{Ca} in DRG neurons from *MrgprX1* mice.

(a) Left: In a control experiment (no blocker, BAM8–22 [BAM] 5 µM) inhibited HVA I_{Ca} by about 50%. Right: N-type HVA calcium channel blocker ω-conotoxin GVIA (1 µM, GVIA) largely abolished BAM8–22-induced HVA I_{Ca} inhibition. **(b)** Left: Without blocker, BAM strongly inhibited HVA I_{ca}. Right: Current-voltage relationship graphs show that ω-agatoxin TK (0.5 µM, TK), a P/Q-type HVA calcium channel blocker, abolished half of BAM8–22-induced HVA I_{ca} inhibition. **(c)** Left: The inhibition of HVA I_{ca} by BAM without blocker. Right: Nimodipine (10 µM), an L-type HVA calcium channel blocker did not reduce BAM8–22-induced HVA I_{ca} inhibition. *n*=5-7 neurons/group.
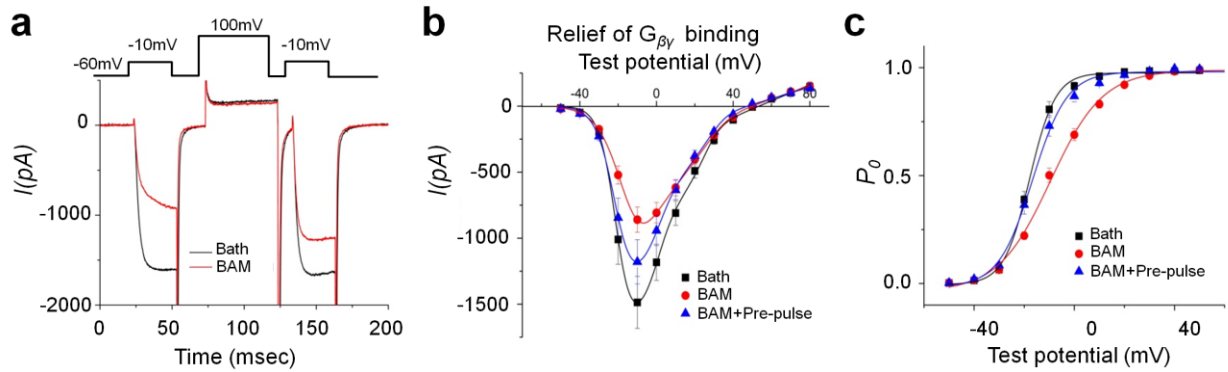
1
2   **SI Appendix, Fig. S4. Inhibition of HVA I_{Ca} by BAM8–22 partially depends on $G_{\alpha i/o}$-**
3   **sensitive $G_{\beta\gamma}$ binding in DRG neurons from *MrgprX1* mice.**

4   **(a)** A representative trace shows the sandwich stimulation protocol used to relieve $G_{\beta\gamma}$
5   binding to the HVA Ca^{2+} channels with and without bath application of BAM8–22 (BAM,
6   5 µM). **(b)** A graph of the current-voltage relationship shows that the depolarizing pre-
7   pulse reversed 50% of BAM8–22-induced inhibition of HVA I_{ca}. **(c)** Open probability
8   shows that the depolarizing pre-pulse reversed the voltage dependence of the channel.
9   *n*=5-6 neurons /group.

10

11
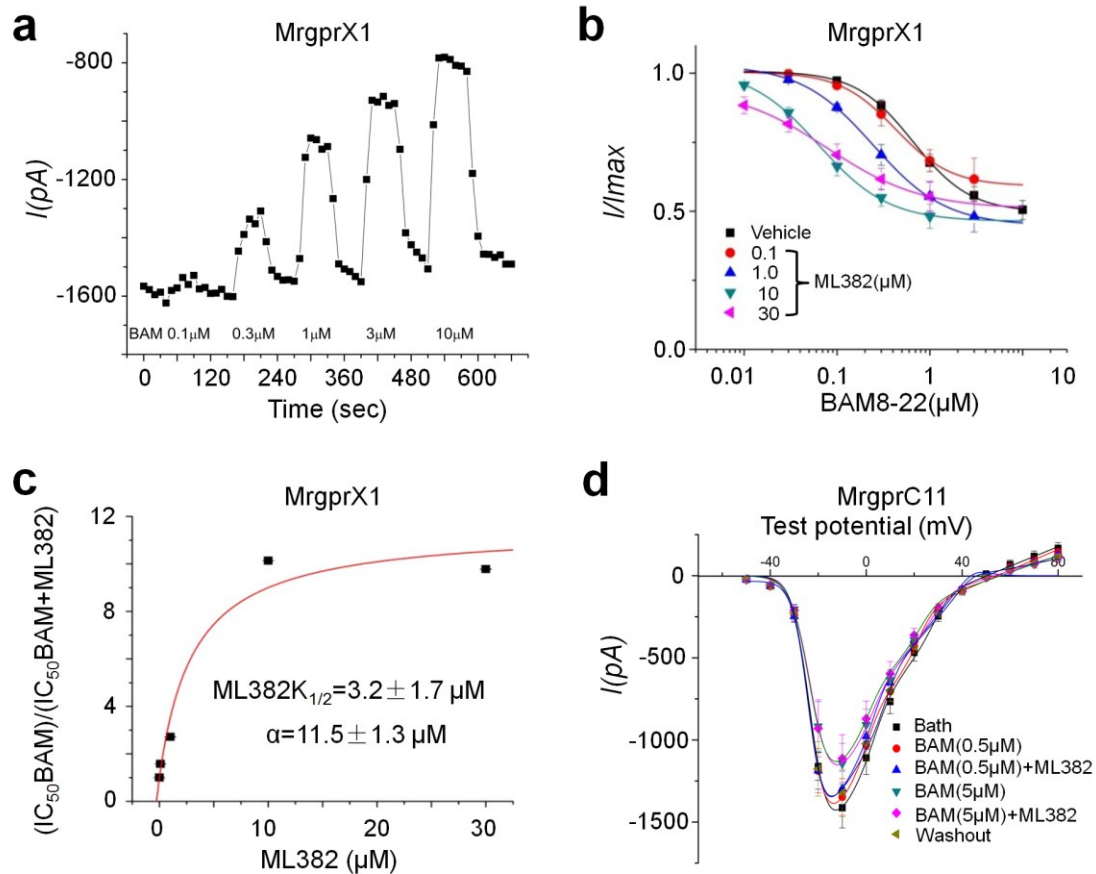
SI Appendix, Fig. S5. Quantification of the potency of ML382 as a positive allosteric modulator for *MrgprX1*.

(a) A representative time course shows the protocol used to measure the dose-response curve of BAM8–22-induced inhibition of HVA I_{ca} in DRG neurons from *MrgprX1* mice. **(b)** IC$_{50}$ of BAM8–22, estimated from the Hill equation in the presence and absence of different concentrations of ML382 (0.1–30 μM) **(c)** The curve used to calculate the EC$_{50}$ and the α value of ML382. **(d)** ML382 did not enhance BAM8–22 inhibition of HVA I_{Ca} through mouse MrgprC11. *n*=6-8 neurons/group.

1

2
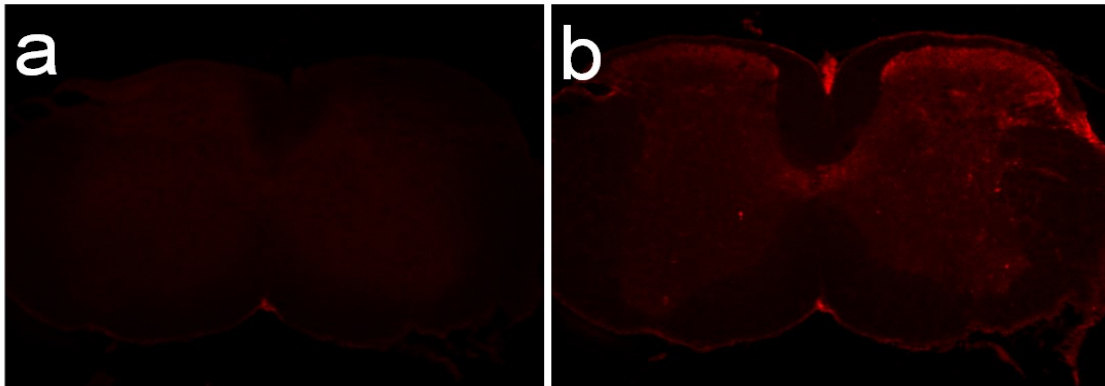
SI Appendix, Fig. S6. Validation of BAM22 antibody.

(a) The anti-BAM22 antiserum was pre-absorbed with 10^{-6} M BAM22, resulting in the absence of BAM22 signal. **(b)** A continuous section of the spinal cord from the same animal was stained with anti-BAM22 antibody that was not pre-absorbed. The BAM22 immunoreactivity is visible on the superficial layers of dorsal horn. The higher signal level on the right side was ipsilateral to the CFA treatment on the hind paw.

9

10

a Low force (0.07g) **b** High force (0.45g)

1
2
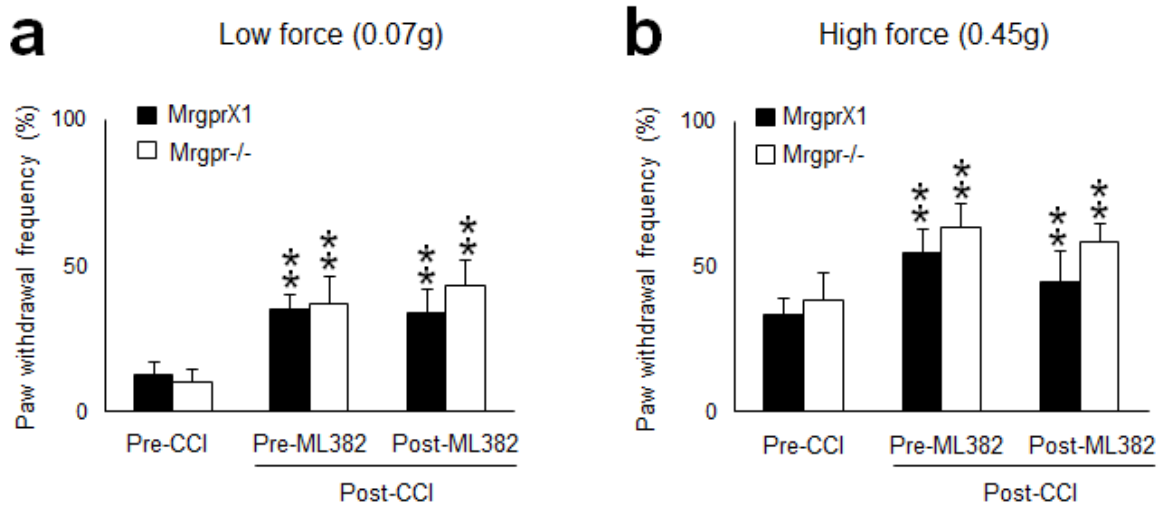
SI Appendix, Fig. S7. Intrathecal injection ML382 did not attenuate mechanical

hypersensitivity in mice after nerve injury.

(a) At 2 weeks after chronic constriction injury (CCI) of the sciatic nerve, the paw

withdrawal frequencies (PWF) to a lower force (0.07g) and **(b)** a higher force (0.45g) von

Frey mechanical stimulation applied to the ipsilateral hindpaw were significantly

increased from the respective pre-injury baselines in MrgprX1 (n=8) and Mrgpr-/-mice

(n=6). Intrathecal administration of ML382 (0.25 mM, 5 µL, i.th.) did not significantly

reduce the increased PWF in response to either low-force or high-force stimuli

regardless of genotype. **P < 0.01 vs pre-CCI, two-way mixed model ANOVA with

Bonferroni *post hoc* test.

13

1
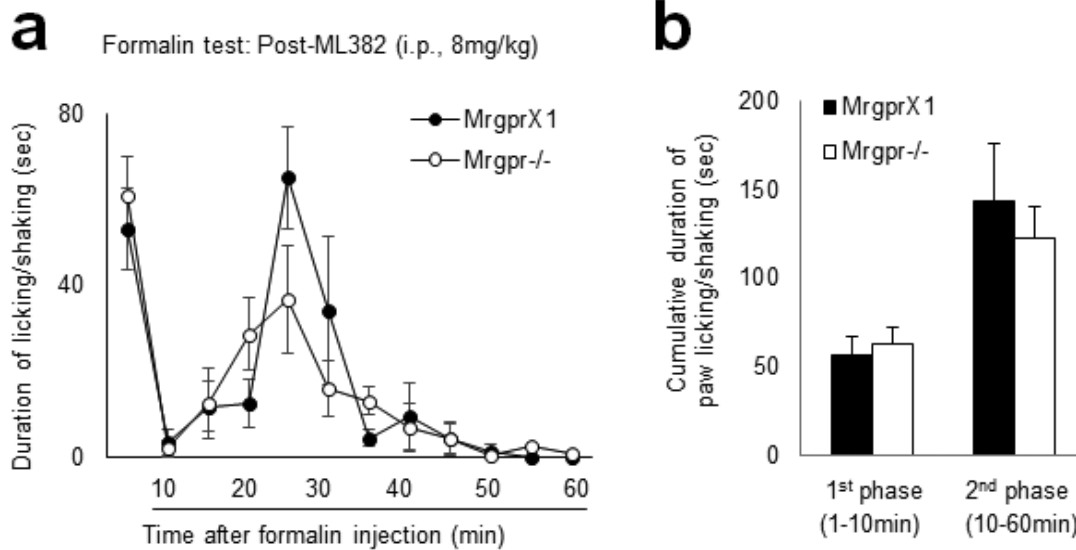
SI Appendix, Fig. S8. Intraperitoneal administration of ML382 did not reduce

formalin-induced pain.

(a) Time course of pain behaviour elicited by intraplantar injection of formalin (2%, 5 µL)

into MrgprX1 and Mrgpr-/- mice that had been pretreated with intraperitoneal injection of

ML382 (8mg/kg, i.p.). **(b)** Cumulative duration of paw licking and shaking after formalin

injection showed that the first and second phases of pain behaviour were not

significantly reduced by ML382 in mice regardless of genotypes. *n*=8/group, two-way

mixed model ANOVA with Bonferroni *post hoc* test.
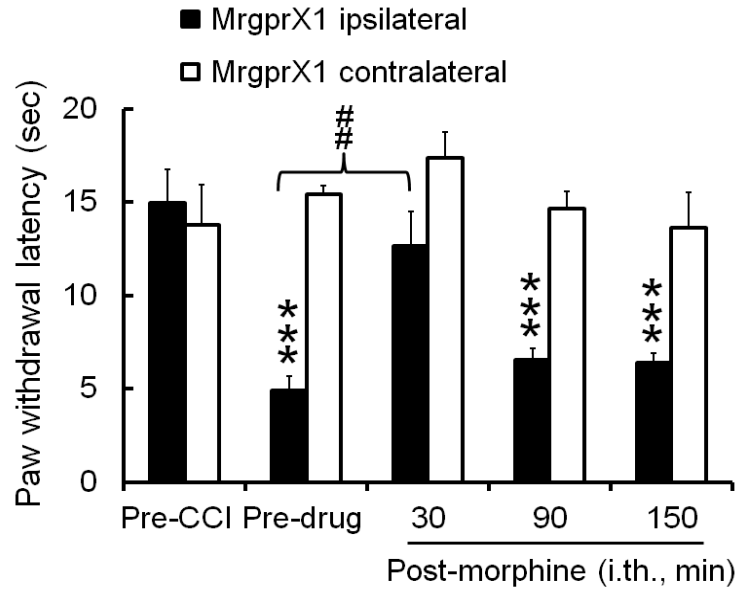
SI Appendix, Fig. S9. Morphine attenuates heat hypersensitivity in MrgprX1 mice after nerve injury.

At 2 weeks after chronic constriction injury (CCI) of the sciatic nerve, the paw withdrawal latency (PWL) to radiant heat stimulation was significantly decreased from pre-injury baseline in the ipsilateral hindpaw of MrgprX1 mice. The heat hypersensitivity in the ipsilateral hindpaw was attenuated at 30 min after an intrathecal administration of morphine (5μl, 1mM, i.th.). Contralateral PWL was not altered by CCI or morphine treatment in MrgprX1 mice. ##$P < 0.01$ vs pre-drug baseline, ***$P < 0.001$ vs pre-CCI, n=8, two-way mixed model ANOVA with Bonferroni *post hoc* test.

Time	Mouse	Rat	Human
0 hr	100%	100%	100%
1 hr	98.47%	102%	103%
4 hr	69.15%	91%	100%

1

2   **Supplemental Table 1. Pharmacokinetic study of ML382.** ML382 was incubated with

3   mouse, rat or human plasma for 0 hr, 1 hr, or 4 hr and then quantified by LC/MC/MC

4   analysis. ML382 was unstable in mouse plasma and stable in rat and human plasma.

1   **SUPPLEMENTAL METHODS**

2   **Reverse transcript PCR**

3   Total RNA was extracted from various tissues using RNeasy Mini Kit (Qiagen) according

4   to the manufacturer's instructions. Reverse transcription was done by Super-Script III

5   First-Strand Synthesis System (Invitrogen). PCR conditions: 95 °C for 3 min, 40 cycles

6   of 30 s at 95 °C, 30 s at 55 °C and 60 s at 72 °C. The primers are located in the human

7   *MrgprX1* exon. The sequence of primers are 5'-TCAACTTGGCCGCAGCAGACTT

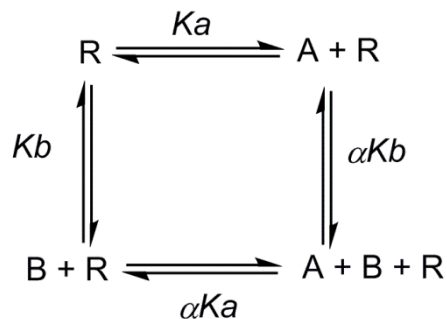8   (forward), 5'-GAGAATCCTGATCAGCAGGACC (reverse).

9   **Analysis of allosterism in functional assay**

10   Dose-response curves were fitted with the Hill equation:

$$E(X) = Emin + \frac{(Emax - Emin) * X^n}{K^n + X^n}$$

11   E(X) is the effect as the function of X (drug concentration). Emin and Emax are

12   the minimum and maximum effects, respectively. K is the equilibrium constant, in this

13   case, the EC_{50}, and n is the Hill coefficient.

14   For mechanistic study of allosteric modulation, a ternary model was used to

15   measure the binding affinity and efficacy of an allosteric modulator. In a ternary complex

16   model with two ligands and one receptor, the interaction within these three molecules

17   can be described with a cyclic model:

$$R \underset{}{\overset{Ka}{\rightleftharpoons}} A + R$$

$$Kb \Big\updownarrow \qquad \Big\updownarrow \alpha Kb$$

$$B + R \underset{\alpha Ka}{\rightleftharpoons} A + B + R$$

1   In this scheme, R is the receptor, A is the orthosteric ligand, and B is the

2   allosteric modulator. Ka and Kb indicate the association constants of ligands A and B,

3   respectively. When both ligands are interacting with the receptor, they each can

4   reciprocally affect the association constants, and the magnitude of this cooperativity is

5   determined by the factor α. The equation that describes the ternary complex model can

6   be derived from the above scheme and is represented by the following:

$$\frac{K}{K'} = \frac{\alpha[B] + Kb}{[B] + Kb}$$

7   K is the dissociation constant of the orthosteric ligand A, K' is the dissociation

8   constant of the ligand A under the influence of the modulator B, and K_b is the

9   dissociation constant of the allosteric modulator B. The details of the ternary complex

10   model and its derivation can be found in the literature (1-3). If the allosteric modulator

11   does not alter maximum efficacy, the dissociation constant K can represent EC_{50} of the

12   ligand, and the equation can be rewritten in the following form (4):

$$\frac{EC50}{EC50'} = \frac{\alpha[B] + Kb}{[B] + Kb}$$

13   **Plasma Protein Binding**

14   Protein binding of ML382 was determined in human, rat and mouse plasma via

15   equilibrium dialysis employing Single-Use RED Plates with inserts (ThermoFisher

1 Scientific, Rochester, NY). Briefly plasma (220 µL) was added to the 96 well plate

2 containing test article (5 µL) and mixed thoroughly. Subsequently, 200 µL of the plasma-

3 test article mixture was transferred to the cis chamber (red) of the RED plate, with an

4 accompanying 350 µL of phosphate buffer (25 mM, pH 7.4) in the trans chamber. The

5 RED plate was sealed and incubated 4 h at 37 °C with shaking. At completion, 50 µL

6 aliquots from each chamber were diluted 1:1 (50 µL) with either plasma (cis) or buffer

7 (trans) and transferred to a new 96 well plate, at which time ice-cold acetonitrile (2

8 volumes) was added to extract the matrices. The plate was centrifuged (3000 rpm, 10

9 min) and supernatants transferred to a new 96 well plate. The sealed plate was stored at

10 -20 °C until LC/MS/MS analysis.

11 **Quantitative analysis of BAM22 peptide in mouse spinal cord by mass**

12 **spectrometry**

13 BAM22 within the mouse spinal cord was quantified by the LC-SRM approach on our

14 optimized MS platform (5). The spinal cords of CFA- and saline-treated mice were

15 homogenized in lysis buffer (PBS, protease inhibitor cocktail from Roche) at 4 °C with

16 0.5 mm glass beads for 5 min in a Bullet Blender instrument (Next Advance Inc.). The

17 whole lysate was mixed with ice-cold acetonitrile at a final concentration of 80% by

18 vortexing at 20-s intervals for 1 min, and then centrifuged at 21,000 x g for 15 min. The

19 extracted lysate was dried before being dissolved and digested with trypsin (2 µg per

20 spinal cord) in 50 mM HEPES (pH 8.5) at 37oC for 5 h. The digests were acidified with 1%

21 TFA, pre-cleared by centrifugation, and desalted with Sep-Pak C18 SPE column

22 (Waters). The BAM22 tryptic peptides were eluted with 45% acetonitrile plus 1% formic

23 acid. The eluted peptides were dried, reconstituted in 5% formic acid, and analysed on

24 Orbitrap Elite hybrid ion trap MS (Thermo Fisher Scientific), equipped with

25 nanoelectrospray ion source and an Easy-nLC 1000 UHPLC system (Thermo Fisher

1   Scientific). Chromatography was performed on a 75 µm x 10 cm picofrit column (New

2   Objective) packed with C18 2.7 µm Halo beads (New Objective). Mobile phases

3   consisted of 0.1% formic acid as solvent A, and 0.1% formic acid/70% acetonitrile as

4   solvent B. The digests were eluted for 20 min at 400 nL/min in a gradient of 30 to 50% B.

5   The LC-SRM was performed with a single Orbitrap MS scan from 350 to 1600 at a

6   resolution of 30,000 with AGC set at 1e5 followed by CID of targeted SRM scans of

7   BAM22 tryptic peptides. For the quantification of BAM22 in mouse spinal cords, the m/z

8   transition of $[M+3H]^{3+}$ precursor ion of $BAM22_{8-19}$ peptide to its product ions was

9   monitored, and the peak areas were calculated by Xcalibur software. Human ubiquitin

10   peptide VGRPEWWMDYQK (100 fmol) was spiked into each run as an internal standard

11   to offset the run-to-run variation. To estimate the absolute amount of BAM22 peptide in

12   the mouse spinal cord, we spiked synthetic BAM22 tryptic digests (250 fmol) into the

13   extracts and analysed them. The peak area of synthetic $BAM22_{8-19}$ peptide was obtained

14   by comparing two runs with or without the spike-in. Relative amounts of BAM22 in CFA-

15   and saline-treated mouse spinal cords were determined by calculating the difference in

16   peak area of multiple SRM transitions of $BAM22_{8-19}$ peptide between the two samples.

17   **Whole-cell voltage-clamp recordings from spinal cord slices.** We used

18   procedures as described previously (48). Briefly, the lumbosacral segment of spinal cord

19   was removed rapidly from CFA-treated MrgprX1 mice or Mrgpr-/- mice and placed in ice-

20   cold, low-sodium Krebs solution (in mM: 95 NaCl, 2.5 KCl, 26 $NaHCO_3$, 1.25 NaH_2PO_4-

21   H_2O, 6 $MgCl_2$, 1.5 $CaCl_2$, 25 glucose, 50 sucrose, 1 kynurenic acid) saturated with

22   95%O_2/5% CO_2. For electrophysiology recording, slices were stabilized with a grid (ALA

23   Scientific, Farmingdale, NY, USA) and submerged in a low-volume recording chamber

24   (SD Instruments, San Diego, CA, USA) that was perfused with room-temperature Krebs

25   solution (in mM: 125 NaCl, 2.5 KCl, 26 $NaHCO_3$, 1.25 NaH_2PO_4-H_2O, 1 $MgCl_2$, 2 $CaCl_2$,

1   and 25 glucose, with 10 µM $GABA_A$ receptor blocker bicuculline and 1 µM glycinergic

2   receptor blocker strychnine) bubbled with a continuous flow of 95% O_2/5% CO_2. Whole-

3   cell patch-clamp recording of lamina II cells was carried out under oblique illumination

4   with an Olympus fixed-stage microscope system (BX51, Melville, NY, USA). Data were

5   acquired with pClamp 10 software (Molecular Devices) and a Multiclamp amplifier. Using

6   a puller (P1000, Sutter, Novato, CA, USA), we fabricated thin-walled glass pipettes

7   (World Precision Instruments) that had a resistance of 3–6 MΩ and were filled with

8   internal solution (in mM: 120 K-gluconate, 20 KCl, 2 $MgCl_2$, 0.5 EGTA, 2 Na_2-ATP, 0.5

9   Na_2-GTP, and 20 HEPES). The cells were voltage clamped at –70 mV. Membrane

10 current signals were sampled at 10 kHz and low-pass filtered at 2 kHz. Larger-bore

11 pipettes filled with Krebs solution were used for dorsal root stimulation. To evoke EPSCs,

12 we delivered paired pulse test stimulation to dorsal root consisting of 2 synaptic volleys

13 (500 µA, 0.1 ms) 400 ms apart at a frequency of 0.05 Hz to activate high-threshold

14 afferent fibres (C-fibres), followed by a 0.1-ms, 5-mV depolarizing pulse (to measure

15 series resistance [R_{series}] and input resistance [R_{input}]). We monitored R_{series} and R_{input} and

16 discarded cells if either of these values changed by more than 20%. The amplitudes of

17 the first (P1) and the second (P2) EPSC were measured, and the paired pulse ratio

18 (PPR) was calculated as PPR = P2/P1.

19 **Immunofluorescence.** For spinal cord staining, adult mice (8–12 weeks old) were

20 anaesthetized with pentobarbital and perfused intracardially with 20 mL of 0.1 M PBS

21 (pH 7.4, 4°C) followed by 25 mL of fixative (4% formaldehyde [vol/vol], 4°C), as

22 previously described (13). Spinal cord was dissected from the perfused mice and post-

23 fixed in fixative at 4°C for 1 h. Then tissues were cryoprotected in 20% sucrose (wt/vol)

24 for 24 h at 4°C and sectioned with a Vibratome cryostat (Polysciences, Warrington, PA).

25 The sections were placed on slides, dried at 37°C for 15 min, and fixed with 4%

paraformaldehyde at room temperature for 10 min. We used Tyramide Signal

Amplification (TSA; PerkinElmer, Waltham, MA) according to the protocol provided. The

sections were incubated with rabbit polyclonal anti-BAM22 antiserum (1:500, ATSBIO,

San Diego, CA, USA) (50) in 1×TNB blocking buffer (0.1 M Tris, 0.15 M NaCl, and 0.5%

[wt/vol] blocking reagent from PerkinElmer) overnight at 4°C, washed, and then

incubated with secondary horseradish peroxidase-conjugated goat anti-rabbit IgG (1:500

in 1×TNB, Vector Laboratories, Burlingame, CA, USA) for 1 h. TSA cyanine 3 reagent

was added for the amplification step. Images were taken with a Carl Zeiss AXIO

Examiner.Z1 confocal microscope (Jena, Germany).

CCI-induced mechanical allodynia

Mechanical sensitivity was assessed with the von Frey test by the frequency method (6).

Two calibrated von Frey monofilaments (low force = 0.07 g; high force = 0.45 g) were

used. Each von Frey filament was applied perpendicularly to the plantar side of each

hind paw for ~1 s; the stimulation was repeated 10 times to both hind paws. The

occurrence of paw withdrawal in each of these 10 trials was expressed as a percent

response frequency: PWF = (number of paw withdrawals/10 trials) × 100%.

Itch behavioural study

Mice were acclimatized 1 day before the test. BAM8–22 or ML382 was injected

subcutaneously into the nape of the neck (50 µL), intraperitoneally (100 µL), or

intrathecally (5 µL). Behavioural responses were video recorded for 30 min. The video

recording was subsequently played back in slow motion, and an investigator counted the

number of bouts of scratching with the hind paw around the injection site.

Motor function test

We used the rotarod test to evaluate whether central administration of ML382

affects motor function as previously described (7). All animals were brought to the

behaviour room 10–20 min before the test. The mice habituated in the rotarod apparatus

(Rotamex, Columbus Instruments) at a constant speed of 4 rpm for 10 min 3–5 times on

day 1. Then, on day 2, they received three acceleration training sessions separated by

20 min. Speeds increased from 4 rpm to 40 rpm (with a 4.0-rpm increase every 30 s).

On day 3, they received three trials before drug administration (in the same acceleration

mode as day 2). Then ML382 was applied intrathecally, without isoflurane. The mice

were tested three times beginning 30 min after drug administration. The end point of the

experiment was defined as the time at which the mice fell from the apparatus or rolled

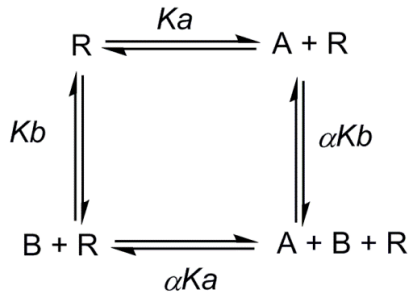over the rod by holding onto it. The latency to the end point was recorded and analysed.

REFERENCES

1. De Lean A, Stadel JM, & Lefkowitz RJ (1980) A ternary complex model explains the agonist-specific binding properties of the adenylate cyclase-coupled beta-adrenergic receptor. *The Journal of biological chemistry* 255(15):7108-7117.
2. Samama P, Cotecchia S, Costa T, & Lefkowitz RJ (1993) A mutation-induced activated state of the beta 2-adrenergic receptor. Extending the ternary complex model. (Translated from eng) *The Journal of biological chemistry* 268(7):4625-4636 (in eng).
3. May LT, Leach K, Sexton PM, & Christopoulos A (2007) Allosteric modulation of G protein-coupled receptors. (Translated from eng) *Annu Rev Pharmacol Toxicol* 47:1-51 (in eng).
4. Ehlert FJ (1988) Estimation of the Affinities of Allosteric Ligands Using Radioligand Binding and Pharmacological Null Methods. (Translated from English) *Mol Pharmacol* 33(2):187-194 (in English).
5. Pagala VR*, et al.* (2015) Quantitative protein analysis by mass spectrometry. *Methods in molecular biology* 1278:281-305.
6. Guan Y*, et al.* (2010) Mas-related G-protein-coupled receptors inhibit pathological pain in mice. (Translated from eng) *Proceedings of the National Academy of Sciences of the United States of America* 107(36):15933-15938 (in eng).
7. Han L*, et al.* (2013) A subpopulation of nociceptors specifically linked to itch. (Translated from eng) *Nature neuroscience* 16(2):174-182 (in eng).

1   **Appendix**

$$R \underset{}{\overset{Ka}{\rightleftharpoons}} A + R$$

(The scheme is a thermodynamic cycle: top row $R \rightleftharpoons A + R$ with Ka; left side Kb; right side αKb; bottom row $B + R \rightleftharpoons A + B + R$ with αKa.)

2

3    $K_a = \dfrac{[AR]}{[A][R]}$

4    $K_b = \dfrac{[BR]}{[B][R]}$

5    $\alpha K_a = \dfrac{[ARB]}{[A][BR]}$

6    $\alpha K_b = \dfrac{[ARB]}{[B][AR]}$

7    $[Rt] = [R]+[AR]+[BR]+[ABR]$

8   Fraction of binding (ρ) $= \dfrac{[AR]+[ABR]}{[R]+[AR]+[BR]+[ABR]}$

9   Since $[AR] = Ka[A][R]$, $[BR] = Kb[B][R]$, $[ABR] = \alpha KaKb[A][B][R]$

10   $\rho = \dfrac{Ka[A][R]+\alpha KaKb[A][B][R]}{[R]+Ka[A][R]+Kb[B][R]+\alpha KaKb[A][B][R]} = \dfrac{[A](1+\alpha Kb[B])}{\frac{1}{Ka}+[A]+\frac{Kb}{Ka}[B]+\alpha Kb[A][B]} = \dfrac{[A](1+\alpha Kb[B])}{[A](1+\alpha Kb[B])+\frac{1+Kb[B]}{Ka}}$

11   $= \dfrac{[A]}{[A]+\frac{1+Kb[B]}{Ka(1+\alpha Kb[B])}}$

12   Dissociation constants $K_A = 1/K_a$ and $K_B = 1/K_b$

13   $\rho = \dfrac{[A]}{[A]+\frac{KA(1+\frac{[B]}{KB})}{1+\frac{\alpha[B]}{KB}}} = \dfrac{[A]}{[A]+KA'}$

1 K_A' is the apparent dissociation constant of [A] in the presence of [B].

2 $K_A' = \dfrac{KA(1+\frac{[B]}{KB})}{1+\alpha\frac{[B]}{KB}} = \dfrac{KA(KB+[B])}{KB+\alpha[B]}$

3 $\dfrac{KA}{KA'} = \dfrac{\alpha[B]+KB}{[B]+KB}$

4